THE JOURNAL OF PHYSICAL CHEMISTRY A

Article

HArF in Solid Argon Revisited: Transition from Unstable to Stable Configuration

Anastasia V. Bochenkova, Vladimir E. Bochenkov, and Leonid Khriachtchev

J. Phys. Chem. A, **Article ASAP** • Publication Date (Web): 25 February 2009

HArF in Solid Argon Revisited: Transition from Unstable to Stable Configuration†

Anastasia V. Bochenkova* and Vladimir E. Bochenkov

Department of Chemistry, M. V. Lomonosov Moscow State University, 1/3 Leninskie Gory, 119991 Moscow, Russian Federation

Leonid Khriachtchev*

Laboratory of Physical Chemistry, P.O. Box 55, FIN-00014 University of Helsinki, Finland

Received: November 28, 2008; Revised Manuscript Received: January 12, 2009

The thermal conversion of HArF configurations in solid argon has been investigated both experimentally and theoretically. The matrix isolation experiments have been concentrated on temperatures 25−27 K, promoting the transition from the unstable to stable HArF configuration. The combined quantum mechanical−molecular mechanical and temperature-accelerated dynamics approach has been developed to study the real-time evolution of HArF trapped in different matrix-site morphologies. Two realistic pathways of the stable HArF formation are found for annealing at 25−27 K. The conversion mechanism in both pathways involves the local mobility of matrix vacancies in the vicinity of the HArF molecule. These two relaxation processes occurring within different timescales can cause the multiexponential decay of unstable HArF observed experimentally. The theoretical values of the activation energy of 64 meV as well as the corresponding pre-exponential factor of exp(28) s^{-1}, obtained for one of the unstable HArF configurations, are well consistent with the experimental estimates of 70 meV and exp(30 ± 3) s^{-1}, respectively.

1. Introduction

Noble-gas (Ng) hydrides with the general formula HNgY constitute a part of modern noble-gas chemistry.[1,2] One representative of this group of molecules is HArF, the first neutral ground-state chemical molecule containing argon. HArF was discovered in 2000 in low temperature argon matrices.[3] This interesting species has later been thoroughly studied computationally.[4−15] In experiments, this compound was first synthesized by using photodissociation of HF in solid argon at 7 K and subsequent annealing at ∼20 K, which promoted the characteristic triplet absorption bands of the H−Ar stretching mode at 1965.7, 1969.4, and 1972.3 cm^{-1}. These bands disappear fast upon annealing above 28 K.[3] It was later observed that HArF exhibits additional blueshifted H−Ar stretching absorptions at 2016.3 and 2020.8 cm^{-1} that corresponded to a solid-state configuration with a larger thermal stability limited only by degrading of the matrix above 40 K.[16] The solid-state HArF configuration with the doublet absorption is called "stable HArF" in order to distinguish it from "unstable HArF" having the triplet absorption around 1970 cm^{-1} and decaying above 28 K. The conversion of the unstable to stable HArF configuration was suggested to occur upon annealing.[16] The low-temperature formation of HArF in solid argon at 7 K was experimentally found and the tunneling mechanism was suggested.[17] The one-to-one interaction of HArF with molecular nitrogen was studied experimentally and computationally, which showed a large complexation-induced blue-shift of the H−Ar stretching frequency.[18]

A number of theoretical works were devoted to the matrix-site geometries of HArF in solid argon. The first attempt to simulate the matrix effect on the vibrational spectrum of HArF was done by Runeberg et al.[5] More extensive simulations confirmed the sensitivity of the H−Ar stretching frequency to local matrix morphology.[19−21] Jolkkonen et al. connected the experimental blue shift of the stable HArF absorption bands with the Ar···HArF complex formed in a loose matrix site.[20] Bochenkova et al. used a quantum mechanical-molecular mechanical approach to simulate several types of trapping configurations of HArF inside the fcc argon lattice. They generally supported Jolkkonen's assignment and moreover found five different morphologies of an argon matrix around HArF molecule and these matrix sites differed by position of a vicinal lattice vacancy.[21] In addition to matrix-site structure, the vibrational spectra of noble-gas hydrides often show a satellite at higher energy from the main H−Ng stretching band. This satellite has a mirror counterpart at a lower frequency rising in intensity at elevated temperatures. These sub-bands were first studied for HXeBr and HKrCl and explained in terms of hindered rotation of the embedded molecule in the matrix.[22] Hindered rotation of HArF in solid argon was studied in detail later.[23] These studies indicate that the band at 1992 cm^{-1} is due to a combination of the H−Ar stretching vibration and hindered rotation.

Despite the previous efforts, details of the mechanism of the decay of unstable HArF and the formation of stable HArF are unclear, and those are the primary goals of the present study. In the present work, we perform additional experiments on HArF in solid argon concentrating on matrix temperatures promoting the HArF configuration conversion. To interpret the experimental observations we develop a theoretical model based on the modified Temperature-Accelerated Dynamics (TAD)[24] specially adjusted for the purposes of the present study. To compute the energies and forces "on-the-fly", the original hybrid Quantum Mechanical/Diatomics-In-Molecules (QM/DIM) approach,[21] which ensures a high accuracy of the nonempirical HArF−Ar interatomic potential, is used. Previously, the QM/DIM potential

† Part of the "Robert Benny Gerber Festschrift".

* To whom correspondence should be addressed. E-mails: leonid.khriachtchev@helsinki.fi, anastasia.bochenkova@gmail.com.

10.1021/jp810457h CCC: $40.75

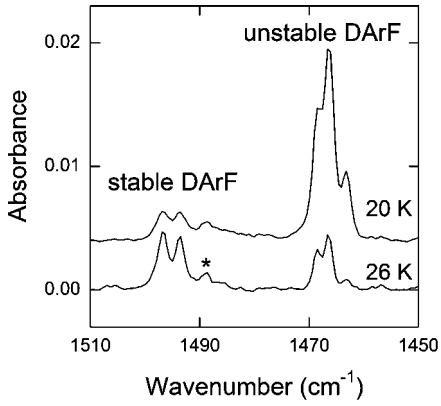

Figure 1. DArF after annealing for 5 min at 20 K and after annealing for 33 min at 26 K. The band marked with an asterisk originates from FOO. The DF/Ar matrix was first photolyzed by a Kr lamp. The spectra were measured at 8 K. The positions of the bands are 1463.2, 1466.3, and 1468.5 cm^{-1} for unstable DArF and 1493.8 and 1496.7 for stable DArF.

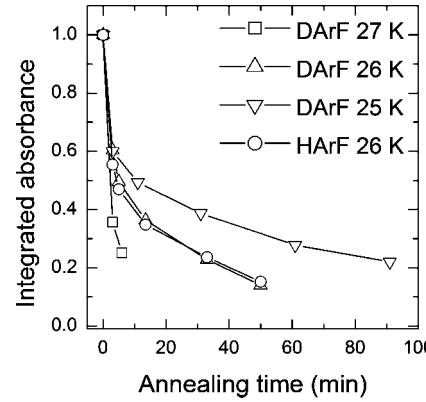

Figure 2. Experimental decay of unstable DArF and HArF at elevated temperatures.

was successfully applied to model trapping sites and absorption bands of HArF in solid argon.[21,23] The present work is aimed at describing the real-time evolution of HArF trapped in different argon matrix sites at experimental temperatures. The developed model provides probable pathways of the HArF configuration conversion upon annealing and sheds light onto geometries of the HArF matrix surrounding.

2. Experimental Results and Experimental Model

The HF/Ar matrices were prepared in a closed-cycle helium cryostat (APD, DE 202A) at temperatures down to 7 K as described elsewhere.[3] The mid-IR absorption spectra were recorded with a Nicolet 60 SX FTIR spectrometer using a resolution of 1 cm^{-1}. The HF/Ar matrixes were quite monomeric with respect to HF as evidenced by the dominating bands at 3962.5 and 3953.8 cm^{-1}.[25] Photolysis of HF was done with a Kr continuum lamp (Opthos) emitting the 127−160 nm light. Some amount of HArF (mainly unstable configuration) is observed already after photolysis indicating the "direct" H + Ar + F → HArF reactions. In particular, this formation of HArF during photolysis shows short-range separation of the dissociating H and F atoms.[26] Annealing at ∼20 K activates formation of unstable HArF and also leads to the appearance of stable HArF. Annealing at ∼30 K bleaches the unstable HArF absorption bands completely and increases the stable HArF concentration. It was previously reported that the increase of deposition temperature from 7 to 18 K shifts the conversion of the configurations to somewhat higher temperatures, approximately from 28 to 31 K.[16] Remarkably, HArF slowly forms in the unstable configuration even at 7 K.[17]

In the present work, we have studied experimentally the decomposition of unstable HArF and the formation of stable HArF at intermediate temperatures from 25 to 27 K. The main experimental observations are illustrated in Figure 1 and Figure 2. These figures present the results mainly for the deuterated molecule DArF, and the case of HArF is similar. The unstable HArF configuration forms fast at 18−20 K. The stable HArF configuration is built in two stages. The first formation stage of stable HArF is observed at ∼20 K together with the unstable configuration whereas the second formation stage requires higher temperatures and is accompanied with the decay of unstable HArF. The decay of unstable HArF and the second formation stage of stable HArF occur with the same rates and temperatures, that is, these seem to be two connected processes. The two spectral components of the stable configuration increase synchronously. On the other hand, the lower-frequency component of the unstable absorptions decreases more efficiently.

The decay kinetics of unstable configuration shows clear temperature dependence in the 25−27 K range. The decay kinetics is not single exponential (stretch exponential), showing a distribution of activation energies, which is typical for solid-state processes. If we measure the decay characteristic time at the 1/e level and prepare the Arrhenius plot, the extracted activation energy is ∼70 meV with the pre-exponential factor of exp(30 ± 3) s^{-1}. However, the initial stage of decay yields smaller activation energy so that these values should be considered with caution. Importantly, the decay curves of unstable DArF and HArF are practically identical, which is consistent with the model of reorganization of the matrix surrounding.[27] The increase of stable configuration is more difficult to analyze; some slower processes occur decreasing its concentration at longer timescales, which may be caused by reactions with mobile matrix species or thermal decomposition of the HArF molecule via the stretching coordinate.

The present and previous experiments on HArF in solid argon suggest the following schematic model. First of all, the reorganization under discussion does not involve global mobility of vacancies.[27] It follows that HF molecules responsible for the HArF formation occupy after deposition single-substitutional sites in an argon matrix. Photodissociation of HF leads to interstitial H and F atoms and the vacancy finds a vicinal position. The closely separated H and F atoms can form HArF in a single-substitutional (tight) site, which is an unstable configuration. In agreement, photolysis produces HArF mainly in the unstable configuration. Moreover, the unstable configuration can be slowly formed at the lowest experimental temperature (7 K), i.e. the H atom can tunnel through the matrix barrier to form HArF without participation of the vacancy.[17,28] Annealing at ∼20 K promotes reactions of the close H + F pair with an Ar atom to produce additional unstable HArF. The triplet band structure of the unstable configuration might originate from discrete positions of the vicinal vacancy with respect to the HArF molecule. Annealing at ∼28 K activates local mobility of vacancies leading to the conversion of the unstable configuration to the stable configuration. As compared with global motion, local (short-range) mobility has weaker energetic restriction.[29] Some amount of stable configuration is seen already after annealing at 20 K, indicating distribution of activation energies for vacancy mobility for different vacancy positions. The conversion of HArF configuration depends on

the deposition temperature, which reasonably indicates a change of the reorganization activation energy for different deposition conditions. Essentially the same process may be discussed in terms of isomerization of HArF in Ar surrounding as a supermolecule. In the following section, we will build a microscopic model consistent with these experimental observations.

3. Computational Details and Results

To model the structural evolution of HArF trapped in an argon matrix, we introduce a novel theoretical methodology based on the accelerated molecular dynamics with the forces calculated on-the-fly from the potential energy surface of the QM/DIM type. Temperature Accelerated Dynamics (TAD) is one of the accelerated molecular dynamics techniques.[30] It has been developed to overcome time limitations of the classical MD method, the applicability of which is unfeasible for the processes occurring on the time scale longer than nanoseconds. This approach is applicable to the systems that are characterized by "infrequent events" when the system makes an occasional transition from one potential basin to another. The transitions are forced to occur more rapidly by increasing the temperature of the system. In each basin, the system is evolved at high temperature during a certain time. Each time when transition out of the basin is detected, the saddle point is determined, the low-temperature waiting time for this transition is estimated, and the trajectory is reflected back into the basin. Such a basin-constrained dynamics provides a list of different pathways with the corresponding activation barriers and waiting times at a low temperature. When this list can be considered as complete, the transition with the shortest waiting time is accepted and the system clock is advanced by this time. The saddle points are located using the climbing image Nudged Elastic Band method (cNEB)[31] and the microscopic rate constants are determined using the harmonic transition-state theory. Finally, the time evolution of the system, that is, the sequence of the visited basin minima connected by the saddle point configurations, is obtained. Recently, TAD has been successfully used in atomistic simulations of vapor-deposited crystal growth at low temperature.[32−35] The experimentally observed decay of the unstable HArF configuration occurs at 25−27 K in an argon matrix on a time scale of seconds and longer. Therefore, the classical MD method is of limited use here whereas TAD is a promising tool to study the formation mechanism of stable HArF.

The energy and forces acting on each atom are calculated as a sum of three types of contributions from the Ar−HArF, Ar−Ar, and HArF interaction potentials:

$$E = E\{\mathrm{HArF}\} + \sum_{i=1}^{n}\sum_{j>i}^{n} E\{\mathrm{Ar}_i\mathrm{Ar}_j\} + \sum_{i=1}^{n} E\{\mathrm{Ar}_i \cdots \mathrm{HArF}\} \quad (1)$$

The Aziz-Chen multiproperty interatomic potential[36] is used to describe the Ar−Ar interaction. The Ar−HArF potential is based on the nonempirical diatomics-in-molecules analytical model[21,37−39] with a balanced treatment of the ionic $(HAr)^+F^-$ and neutral HArF configurations through the first order intermolecular perturbation theory.[40] The HArF molecule is treated at the MP2/6−311++G(2d,2p) level of theory validated in the previous studies.[21] The Aziz-Chen and DIM potentials have been implemented in the TAD source code, and the quantum mechanical calculations have been performed in parallel by using PC GAMESS[41] computational package with an efficient implementation of the MP2 gradient code invoked automatically by TAD.

To locate stationary points on the QM/DIM potential energy surface, the consistent iterative procedure is implemented into the TAD code.[21,39] The computational scheme is performed as a series of full and constrained geometry searches within a two-step algorithm, combining a conventional quasi-Newton step in the full 3N-dimensional Cartesian configurational space and Newton steps in the reduced subspace with the frozen geometry of the HArF molecule. The algorithm is repeated until the gradient convergence criteria in full configurational space are fulfilled. With analytical evaluation of the force constant matrix, the optimization in a reduced coordinate subspace refers to the most efficient Newton algorithm of the second order. The consistency of this procedure is reached in the full configurational space with an explicit analytical force constant matrix evaluation for the HArF/Ar interface region. The geometries of the saddle points found by the cNEB algorithm have been further refined by using the quadratic approximation approach,[42] which explicitly uses the information of the negative curvature of the potential energy surface near the transition state. All stationary points are validated to be either a transition state or a true minimum by performing the vibrational analysis.

The argon matrix is represented by a slab of the fcc lattice with 4 × 4 × 4 unit cells of 362 Ar atoms and the HArF molecule trapped in the central cubooctahedral cage. The positions of the outer Ar atoms are kept fixed during the dynamics to prevent thermal expansion of the system at high temperatures, 250 and 350 K, used in the current work. The values of low temperature (25−30 K) correspond to the experimental conditions, at which the unstable HArF configuration is converted to the stable one. The temperature is controlled using the Langevin thermostat. The 1 fs MD time step is used for the accurate treatment of the H atom movement.

The initial structures for the QM/DIM/TAD simulations correspond to the unstable HArF configurations in solid argon (see Figure 3a). They originate from the C_{4v} geometry with different distribution of vacancies around the HArF molecule. Figure 3b illustrates the stable HArF configuration with the C_{2v} symmetry. These configurations are the true minima on the hybrid QM/DIM potential energy surface as found previously.[21] The first and second cuboctahedral solvation outer-shells that are most important for the present consideration contain 12 and 42 Ar atoms. The second outer-shell consists of three sets of symmetry-equivalent atoms. These different sets correspond to a certain topological site in the polyhedron: face, edge and vertex, with the numbers of atoms in each subshell being equal to 6, 24, and 12, respectively, the sets being listed in the order of increasing distance from the central Ar atom of the HArF molecule. The results of the QM/DIM/TAD simulation allow to determine several types of reorganizations with different characteristic times. In particular, the vicinal vacancy can move in the first and second solvation shells and exchange between the first and second shells, and the HArF molecule can rotate inside the matrix. The vacancy movement is equivalent to a jump of a neighboring Ar atom in the opposite direction. The relative energies of initial and final states as well as energy barriers of all transitions are summarized in Figure 4 and Table 1.

The highest energy unstable configuration, which is characterized by the presence of a vacancy in the first solvation shell, undergoes the fastest decay at 25 K with an energy barrier E_a of 41 meV. This configuration is denoted as $Vac^1(Ar)$ in Figure 3a. In this process, the vacancy moves in the first solvation shell to the position near the F atom. Such a configuration does not correspond to a minimum on the potential energy surface,

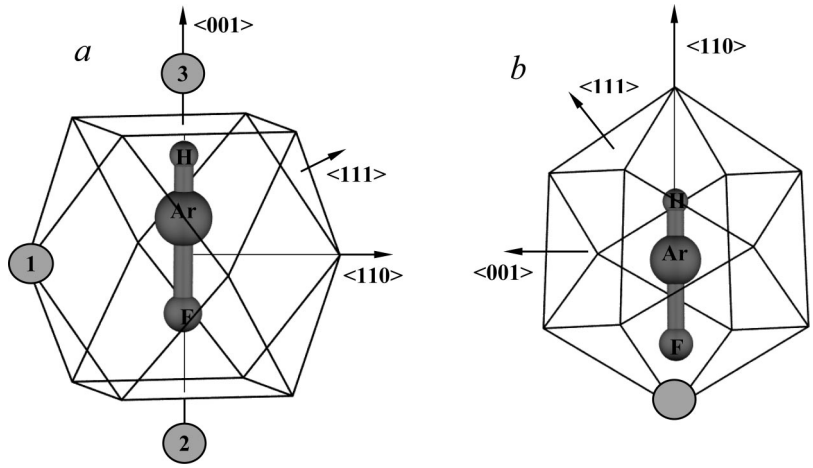

Figure 3. Trapping site structures of HArF in solid argon. The first solvation shell consisting of 12 or 11 nearest neighbor atoms is shown. The vacancies are marked with shaded circles. The possible orientations of HArF in three directions are depicted as ⟨001⟩ (four-atomic window), ⟨110⟩ (nearest neighbor), and ⟨111⟩ (three-atomic window). (a) Unstable HArF configurations with the C_{4v} local symmetry; vacancy positions in the initial configurations: 1, $Vac^1(Ar)$; 2, $Vac^{2ax}(F)$; 3, $Vac^{2ax}(H)$. (b) Stable HArF configuration with the C_{2v} symmetry, $Vac^1(F)$.

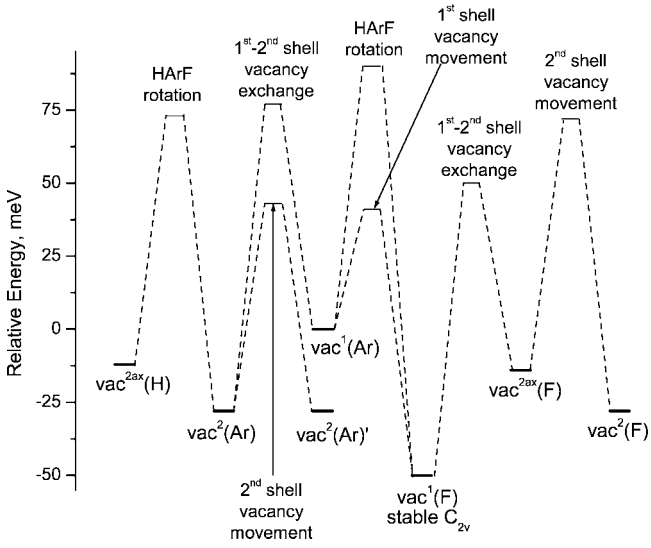

Figure 4. Energy diagram of HArF configurations in solid argon. Energy minima are depicted with bold lines, transition states are depicted with thin lines. All minima refer to the unstable configurations, except the stable configuration $Vac^1(F)$.

TABLE 1: Relative Energies ΔE and Energy Barriers E_a of Transitions (in meV) Found in the QM/DIM/TAD Simulations

initial state	final state	ΔE	E_a	E_a reverse
	1st shell vacancy movement			
$Vac^1(Ar)$unstable	$Vac^1(F)$stable	−50	41	91
	1st−2nd shell vacancy exchange			
$Vac^{2ax}(F)$unstable	$Vac^1(F)$stable	−36	64	100
$Vac^1(Ar)$unstable	$Vac^2(Ar)$unstable	−28	77	105
	2nd shell vacancy movement			
$Vac^2(Ar)$unstable	$Vac^2(Ar)'$unstable	0	71	71
$Vac^{2ax}(F)$unstable	$Vac^2(F)$unstable	−14	85	100
	HArF rotation			
$Vac^{2ax}(H)$unstable	$Vac^2(Ar)$unstable	−16	85	101
$Vac^1(Ar)$unstable	$Vac^1(F)$stable	−50	90	140

leading to the barrierless transition to the stable configuration accompanied with a small-angle rotation of the HArF molecule. The final configuration is denoted as $Vac^1(F)$ in Figure 3b. The average lifetime of this initial state $Vac^1(Ar)$ at 25 K is only a few milliseconds. This is the fastest pathway for the transition to the stable configuration, and the energy barriers of other pathways are at least 1.5 times higher.

The second pathway for the formation of stable HArF configuration occurs on a different time scale. This process corresponds to the movement of the vacancy, which is initially located in the face subshell of the second solvation shell near the F atom [$Vac^{2ax}(F)$ in Figure 3a]. This vacancy can move into the first solvation shell to the position near the F atom, which is followed by the barrierless transition to the stable configuration. The average lifetime of this initial state at 25 K is of the order of seconds, and the activation energy of the process is 64 meV.

The energy barriers for the vicinal vacancy movement drastically depend on its position with respect to the HArF molecule. The differences can be seen in the second solvation shell. In particular, the activation energy values for the second shell vacancy movements are in the range of 71−100 meV (see Table 1). The lowest energy process includes the vacancy movement in the edge subshell of the second solvation shell between the isoenergetic $Vac^2(Ar)$ and $Vac^2(Ar)'$ configurations. For the second initial state $Vac^{2ax}(F)$, the face-edge in-shell vacancy movements to the $Vac^2(F)$ configuration require higher activation energy than the vacancy inclusion into the first solvation shell near the F atom with the formation of the stable $Vac^1(F)$ configuration. The activation energies for these processes are 85 and 64 meV, respectively, meaning that the former process is much slower. When the vacancy comes to the first solvation shell, the stable configuration rapidly forms.

The third initial state of unstable HArF [$Vac^{2ax}(H)$ in Figure 3a] undergoes the transition to other types of unstable HArF configurations with a vacancy located in the second solvation shell. For this initial state the interconversion of unstable configurations $Vac^{2ax}(H)$ and $Vac^2(Ar)$ involves the HArF rotation inside the matrix and it is characterized by high activation energies above 85 meV. This initial unstable state should not lead to the efficient formation of stable HArF at experimental temperatures. However, the total conversion of all unstable HArF configurations to the stable ones is observed in the experiment. It follows that the unstable $Vac^{2ax}(H)$ configuration should not form under experimental conditions. This fact can be rationalized in terms of the relative probabilities of vicinal vacancy formation near the H or F atoms of the HArF molecule upon annealing at 20 K after photolysis. The prob-

ability to occupy a "pure" interstitial position after HF photolysis is higher for the H atom due to its larger mobility compared to the heavier F atom.

An alternative mechanism of the formation of stable HArF could be rotation of a trapped molecule inside the cavity without vacancy assistance. However, the calculations clearly show that these events are improbable at the experimental temperatures. The computed activation energy of this process is 90 meV (see Table 1). It is consistent with the experimental results, which indicate the surrounding reorganization mechanism.

The experimentally observed decay of the unstable HArF configurations exhibits a nonsingle-exponential behavior, and the initial stage of decay yields a small activation energy. Based on the results of the QM/DIM/TAD simulation, the two components of the decay kinetics can be ascribed to the independent transitions of the unstable configurations originated from the different positions of the vicinal vacancy with respect to the HArF molecule. It should be noted that the absolute values of the energy barriers should be considered with caution. These values are expected to be underestimated in the present simulations mainly because of the empirical Aziz-Chen Ar−Ar interaction potential. To justify the latter statement we point out that the use of the Aziz-Chen potential in the simulations of the vacancy diffusion in solid argon results in the activation energy of 80 meV, which is twice smaller than the experimental value (160−170 eV).[43] However, the accuracy of the present studies of the HArF matrix site evolution is expected to be much higher since the most important contributions to the total energy come from the nonempirical DIM interaction potential, which adequately describes the whole configurational space of each Ar−HArF pair. Assuming that the final absolute values of activation energies are somewhat underestimated, the energy barriers of the two most probable pathways of the unstable HArF decay can be in the range of 41−61 and 64−84 meV. These values give the average lifetime of the order of seconds and a few hours for the corresponding initial unstable structures at 25 K. The increase of temperature to 27 K shortens the lifetime of the long-lived component to half an hour. These theoretical estimates are consistent with the experimental data (see Figure 2). The theoretical pre-exponential factor corresponding to the barrier of 64 meV is exp(28) s^{-1}, which agrees well with the experimental value of the pre-exponential factor of exp(30 ± 3) s^{-1} and the activation energy of about 70 meV.

4. Concluding Remarks

We have presented the experimental and theoretical analysis on the decomposition of the unstable HArF configuration leading to the formation of the stable HArF configuration in solid argon at temperatures from 25 to 27 K. The mechanism proposed for the conversion involves the local mobility of a vicinal vacancy, as follows from both experimental and theoretical results. An alternative mechanism of the formation of stable HArF by the rotation of the trapped molecule inside the matrix cavity without vacancy assistance is energetically improbable at the experimental temperatures.

The multiexponential decay kinetics found experimentally at 25−27 K can be ascribed to several independent processes characterized by different activation energies, and hence occurring on different timescales. The proposed initial states correspond to two unstable configurations with the C_{4v} local symmetry and distinct location of the vicinal vacancy with respect to the HArF molecule. The short-lived component in the decay kinetics is connected to the decomposition of the unstable HArF configuration with the vacancy in the first solvation shell, while the longer-lived configuration has a vacancy in the second solvation shell. In the former case the activation barrier is determined by the vacancy movement in the first solvation shell. In the latter case, the conversion is limited by the transition of the vacancy from the second to the first solvation shell, which has higher activation energy. Furthermore, the activation energy for vacancy mobility depends drastically on the vacancy position. The obtained activation energies are in the wide range of 41−105 meV. The computational values of the energy barriers should be considered with caution because they are probably underestimated, which may in principle influence the exact scenario of solid-state reorganization.

It is shown experimentally that the stable HArF configuration is formed in two stages, with the first stage coming at ∼20 K together with the unstable HArF configuration. This observation can be explained either by the formation of some amount of stable HArF directly from the atoms or/and by initial formation of some unstable HArF configuration with the vacancy located in the first solvation shell near the F atom, which undergoes the barrierless transition to the stable structure by a small angle rotation of the HArF molecule inside the cavity.

The second formation stage of stable HArF is presumably connected with the decomposition of unstable HArF because the absorptions of stable HArF correlate in experiment with the decrease of the absorptions of unstable HArF. The two absorption bands of stable HArF increase synchronously indicating that this doublet comes from similar geometries with respect to the vicinal vacancy position. On the other hand, the low frequency component in the triplet of unstable HArF decreases more efficiently than the other two components and can be traced to a different unstable configuration. Therefore the triplet structure originates from at least two unstable configurations, which differs by the vicinal vacancy position. Based on the calculations, the initial unstable configuration $Vac^{1}(Ar)$ may be associated with the short-lived component in the decay kinetics undergoing fast conversion at 25−27 K while the $Vac^{2ax}(F)$ configuration may corresponds to slower decay components.

It is worth mentioning that temperature-accelerated dynamics is applied for the first time here to study the real-time dynamics of matrix-isolated species. Well beyond the present application, this approach is promising to study various solid-state processes at the atomistic level within real experimental timescales. When combined with the *ab initio* or hybrid quantum mechanical-molecular mechanical potentials, it will also allow to model diffusion-controlled chemical reactions in solid matrices; in particular, the formation of HArF upon annealing at 20 K.

Acknowledgment. The work was supported by the Academy of Finland through the Finnish Center of Excellence "Computational Molecular Science" and the Russian Foundation for Basic Research (Project 08-03-00712). We are grateful to A. Voter for the original TAD source code and A. V. Nemukhin for reading and commenting the manuscript.

References and Notes

(1) Khriachtchev, L.; Räsänen, M.; Gerber, R. B. *Acc. Chem. Res.* **2009**, *42*, 183.

(2) Grochala, W. *Chem. Soc. Rev.* **2007**, *36*, 1632.

(3) Khriachtchev, L.; Pettersson, M.; Runeberg, N.; Lundell, J.; Räsänen, M. *Nature (London)* **2000**, *406*, 874.

(4) Lundell, J.; Chaban, G. M.; Gerber, R. B. *Chem. Phys. Lett.* **2000**, *331*, 308.

(5) Runeberg, N.; Pettersson, M.; Khriachtchev, L.; Lundell, J.; Räsänen, M. *J. Chem. Phys.* **2001**, *114*, 836.

(6) Chaban, G. M.; Lundell, J.; Gerber, R. B. *Chem. Phys. Lett.* **2002**, *364*, 628.
(7) McDowell, S. A. C. *Chem. Phys. Lett.* **2003**, *377*, 143.
(8) McDowell, S. A. C. *J. Chem. Phys.* **2003**, *118*, 4066.
(9) McDowell, S. A. C. *Phys. Chem. Chem. Phys.* **2003**, *5*, 808.
(10) Li, H.; Xie, D.; Guo, H. *J. Chem. Phys.* **2004**, *120*, 4273.
(11) Yen, S.-Y.; Mou, C.-H.; Hu, W.-P. *Chem. Phys. Lett.* **2004**, *383*, 606.
(12) Avramopoulos, A; Reis, H.; Li, J.; Papadopoulos, M. G. *J. Am. Chem. Soc.* **2004**, *126*, 6179.
(13) Chen, Y.-L.; Hu, W.-P. *J. Phys. Chem. A* **2004**, *108*, 4449.
(14) Lignell, A.; Khriachtchev, L.; Lundell, J.; Tanskanen, H.; Räsänen, M. *J. Chem. Phys.* **2006**, *125*, 184514.
(15) Li, T.-H.; Liu, Y.-L.; Lin, R.-J.; Yeh, T.-Y.; Hu, W.-P. *Chem. Phys. Lett.* **2007**, *434*, 38.
(16) L. Khriachtchev, L.; Pettersson, M; Lignell, A.; Räsänen, M. *J. Am. Chem. Soc.* **2001**, *123*, 8610.
(17) Khriachtchev, L.; Lignell, A.; Räsänen, M. *J. Chem. Phys.* **2005**, *123*, 064507.
(18) Lignell, A.; Khriachtchev, L.; Pettersson, M.; Räsänen, M. *J. Chem. Phys.* **2003**, *118*, 11120.
(19) Bihary, Z.; Chaban, G. M.; Gerber, R. B. *J. Chem. Phys.* **2002**, *116*, 5521.
(20) Jolkkonen, S.; Pettersson, M.; Lundell, J. *J. Chem. Phys.* **2003**, *119*, 7356.
(21) Bochenkova, A. V.; Firsov, D. A.; Nemukhin, A. V. *Chem. Phys. Lett.* **2005**, *405*, 165.
(22) Khriachtchev, L.; Lignell, A.; Juselius, J.; Räsänen, M.; Savchenko, E. *J. Chem. Phys.* **2005**, *122*, 014510.
(23) Bochenkova, A. V.; Khriachtchev, L.; Lignell, A.; Räsänen, M.; Lignell, H.; Granovsky, A. A.; Nemukhin, A. V. *Phys. Rev. B* **2008**, *77*, 094301.
(24) Sørensen, M. R.; Voter, A. F. *J. Chem. Phys.* **2000**, *112*, 9599.
(25) Anderson, D. T.; Winn, J. S. *Chem. Phys.* **1994**, *189*, 171.
(26) Khriachtchev, L.; Pettersson, M.; Lundell, J.; Räsänen, M. *J. Chem. Phys.* **2001**, *114*, 7727.
(27) Khriachtchev, L.; Lignell, A.; Räsänen, M. *J. Chem. Phys.* **2004**, *120*, 3353.
(28) Bihary, Z.; Chaban, G. M.; Gerber, R. B. *J. Chem. Phys.* **2003**, *119*, 11278.
(29) Khriachtchev, L.; Pettersson, M.; Pehkonen, S.; Isoniemi, E.; Räsänen, M. *J. Chem. Phys.* **1999**, *111*, 1650.
(30) Voter, A. F.; Montalenti, F.; Germann, T. C. *Annu. Rev. Mater. Res.* **2002**, *32*, 321.
(31) Henkelman, G.; Uberuaga, B. P.; Jónsson, H. *J. Chem. Phys.* **2000**, *113*, 9901.
(32) Montalenti, F.; Sorensen, M. R.; Voter, A. F. *Phys. Rev. Lett.* **2001**, *87*, 126101.
(33) Montalenti, F.; Voter, A. F. *Phys. Rev. B* **2001**, *64*, 081401.
(34) Montalenti, F.; Voter, A. F. *Phys. Stat. Sol. (b)* **2001**, *226*, 21.
(35) Sprague, J. A.; Montalenti, F.; Uberuaga, B. P.; Kress, J. D.; Voter, A. F. *Phys. Rev. B* **2002**, *66*, 205415.
(36) Aziz, R. A.; Chen, H. H. *J. Chem. Phys.* **1977**, *67*, 5719.
(37) Tully, J. C. In *Modern Theoretical Chemistry, Semiempirical Methods of Electronic Structure Calculation*; Segal, G. A., Ed.; Plenum Press: New York, 1977; p 173.
(38) Grigorenko, B. L.; Nemukhin, A. V.; Apkarian, V. A. *J. Chem. Phys.* **1996**, *104*, 5510.
(39) Bochenkova, A. V.; Suhm, M. A.; Granovsky, A. A.; Nemukhin, A. V. *J. Chem. Phys.* **2004**, *120*, 3732.
(40) Buchachenko, A. A.; Stepanov, N. F. *J. Chem. Phys.* **1996**, *104*, 9913.
(41) Granovsky, A. A. PC GAMESS, http://classic.chem.msu.su/gran/gamess/index.html.
(42) Culot, P.; Dive, G.; Nguyen, V. H.; Ghuysen, J. M. *Theoret. Chim. Acta* **1992**, *82*, 189.
(43) Simmons, R. O. *Mater. Chem. Phys.* **1997**, *50*, 124.

JP810457H